fibers

MDPI

Article

Influence of Draw Ratio and Take-Up Velocity on Properties of Ultrafiltration Hollow Fiber Membranes from Polyethersulfone

George Dibrov [1,*], George Kagramanov [1], Vladislav Sudin [2], Sergey Molchanov [3], Evgenia Grushevenko [3], Alexey Yushkin [3] and Vladimir Volkov [3,*]

[1] Department of Membrane Technology, D. Mendeleev University of Chemical Technology of Russia, 125047 Moscow, Russia; kagramanov.g.g@muctr.ru
[2] Baikov Institute of Metallurgy and Materials Science, Russian Academy of Sciences, 119334 Moscow, Russia; sudin.vlad@gmail.com
[3] A.V. Topchiev Institute of Petrochemical Synthesis RAS, Russian Academy of Sciences, 119071 Moscow, Russia; spmolchanov@ips.ac.ru (S.M.); evgrushevenko@ips.ac.ru (E.G.); halex@ips.ac.ru (A.Y.)
* Correspondence: dibrov.g.a@muctr.ru (G.D.); vvvolkov@ips.ac.ru (V.V.); Tel.: +7-495-6475927 (ext. 293) (G.D.); +7-915-2119477 (V.V.)

Abstract: This study aimed to reveal the influence of the draw ratio and take-up speed on the pore size distribution and morphology of the hollow fiber ultrafiltration membrane selective layer. To this end, spinnerets with ring ducts of 1.8 and 1.3 mm were employed, whereas the external diameter of the obtained fiber was kept equal. Atomic force microscopy and scanning electron microscopy were employed to study the morphology of the selective layer. Liquid–liquid displacement porosimetry was used to determine the limiting pore size distribution. The produced polyethersulfone ultrafiltration membranes had a robust, sponge-like porous structure, permeance 1000 L/(m^2·h·bar), smooth selective layer, and mean pore size 25 nm. It was found that limiting pore sizes are affected more by the change in the take-up speed, whereas the surface pore sizes, roughness, and morphology are controlled by the draw ratio. It was shown that excessive draw causes the selective layer stretching and crop-up of the porous sublayer. Consequently, the diameters of the spinneret ring duct and the bore needle should match the hollow fiber outer and lumen diameters, respectively.

Keywords: polyethersulfone; hollow fiber; membrane; draw ratio; take-up velocity; ultrafiltration; roughness; morphology

Citation: Dibrov, G.; Kagramanov, G.; Sudin, V.; Molchanov, S.; Grushevenko, E.; Yushkin, A.; Volkov, V. Influence of Draw Ratio and Take-Up Velocity on Properties of Ultrafiltration Hollow Fiber Membranes from Polyethersulfone. *Fibers* **2022**, *10*, 29. https://doi.org/10.3390/fib10030029

Academic Editor: Carlo Santulli

Received: 17 January 2022
Accepted: 9 March 2022
Published: 17 March 2022

1. Introduction

Asymmetric ultrafiltration (UF) hollow fiber membranes are often made employing the nonsolvent-induced phase separation process (NIPS). This technique is among the first to be commercially explored and is one of the most popular membrane formation methods because it allows the preparation of many membrane morphologies, tailored for a specific separation. The method includes immersion of a dope (polymeric) solution into a coagulation bath. The polymer membrane solidifies through the exchange of the solvent and nonsolvent; hence, the solvent–nonsolvent system must be miscible [1].

Ultrafiltration can remove the finest particles found in the water supply, with the removal rating dependent upon the pore size of the selective (dense, skin) layer of the membrane. Generally, the selective layer of such membranes is located at the lumen side of the hollow fiber with the inside-out filtration mode. The main features of the selective layer, affecting the separation performance of the UF membrane are the porosity, pore size distribution, surface roughness and morphology, and contact angle. All these features, and the separation performance, respectively, are determined and can be set by the following spinning conditions:

- Composition and temperature of the spinning dope solution and bore fluid [1–7];
- Dope and bore liquid flow rate and the take-up velocity [8–13];

- Air-gap height [11,14];
- Spinneret design [8,15];
- Draw ratio [16].

It has been suggested that different flow patterns of shear flow and elongation flow are exhibited inside the spinneret and in the air gap, respectively [17]. The elongation basically stretches the polymer chains and enhances the chain packing in the selective layer of hollow fiber membranes, whereas the shear mainly aligns the polymer chains [18]. When the dope extrusion speed increased, pore size and water permeability decreased, but the rejection increased [10]. In one study [9], the authors concluded that a higher dope flow rate (shear rate) in the spinneret resulted in a hollow fiber UF membrane with a smaller pore size and a denser selective layer due to a greater molecular orientation.

Few studies were devoted to the influence of draw ratio on the properties of hollow fiber membranes. The draw ratio (*DR*) is the ratio of the take-up velocity, V_t, and average dope extrusion velocity, V_d. This parameter is defined as

$$DR = \frac{V_t}{V_d} = \frac{V_t \pi \left(D_1^2 - D_2^2\right)}{4Q_d} \quad (1)$$

where Q_d is the volumetric dope extrusion rate. D_1 and D_2 define the dope annular cross-section leaving the spinneret. The take-up velocity is established by the speed of a take-up wheel.

In [16], polysulfone hollow fibers were spun at different draw ratios by varying the speed of the take-up wheel. With a rise in the draw ratio the fiber wall thickness decreased, which was accompanied by the reduction of He/CO_2 selectivity and a rise in gas permeance. In [15], five different spinnerets were employed to obtain Torlon gas separation membranes. The outer diameter was increased by 0.4 mm in sequence, whereas a similar ratio of outer-to-inner diameters was maintained. The effect of draw ratio and spinneret geometry was studied on O_2/N_2 separation performance, although the difference in wall thickness was not taken into account.

The influence of draw ratio and take-up velocity on the morphology of the UF membrane selective layer has not been studied. However, it is clear that the selective layer surface morphology is essential for the improvement of anti-fouling properties [19]. A smoother surface is generally supposed to endure less fouling because polluting particles are expected to be entrapped by rougher surfaces than by smoother surfaces [20]. Mathematical modeling using DLVO interaction energy between fouling particles and rough membrane surfaces implies that as particles approach closer to the membrane, they are more likely to be trapped in the valleys of the rough membrane [21]. In [22], it was shown that the membrane with a dense skin layer showed higher permeability and greater permeability recovery by backwashing. In a few studies [23,24], it was revealed that more fouling particles were concentrated in the valley between the ridges of the separating layer, while the top of the ridges was kept clean.

The focus of this research was to reveal the influence of draw ratio and take-up speed on the selective layer morphology and pore size distribution. The draw ratio was varied by altering the spinneret ring duct diameter while keeping fiber geometry constant. To this effect, polyethersulfone UF membranes were obtained with the selective layer at the lumen side of the fiber.

2. Materials and Methods

2.1. Materials

Polyethersulfone (PES) Ultrason S6020P natural (M_w = 75 kDa) and polyvinylpyrrolidone (PVP) Luvitec K90 (M_w = 1400 kDa) were supplied by BASF (Germany). The following reagents were employed in this study: polyethylene glycol 200 (PEG-200, Forward Group, Russia), ethanol (EtOH, 95%, Spirtmed, Russia). Reverse osmosis water with a specific conductivity of no more than 30 μS/cm was produced on-site. The following

extra pure reagents (>99.5%), provided by CHIMMED, Russia were employed: N,N-dimethylformamide (DMF), isobutanol (BuOH), and sodium bisulfate.

2.2. Asymmetric Hollow Fiber Spinning and Characterization

The NIPS process was used to obtain asymmetric hollow fiber membranes from polyethersulfone [25]. Water is the cheapest and most frequently used coagulation media employed for this purpose. With this in mind, all of the dope solvents need to have good solubility in water. The solubility parameter distance (R_a) was used to quantify the quality of the solvent using the following formula:

$$R_a = \sqrt{4(\delta_{d2} - \delta_{d1})^2 + (\delta_{p2} - \delta_{p1})^2 + (\delta_{h2} - \delta_{h1})^2} \quad (2)$$

In the group of commonly used water-soluble solvents, DMF was chosen, because it has a low value of R_a (Table 1) and is a cheaper solvent than NMP and DMAc. Polyethyleneglycols are often applied as nonsolvents due to their good pore-forming properties [5,26]. In [27], PEG-400 was chosen as a weak nonsolvent, and water was used as a strong nonsolvent. With such composition, the highest reported air-gap distance was 16 cm, which sometimes may be inconvenient and limits the study of the air-gap influence on properties of the hollow fiber. Moreover, water has relatively high vapor pressure, which may create a layer of coagulated polymer on top of the dope solution. Using PEG-200, which is a stronger nonsolvent than PEG-400 (Table 1), allowed to exclude water from the dope solution. Polyvinylpyrrolidone K-90 was used to increase the solution viscosity, membrane porosity, and hydrophilicity.

Table 1. Hansen solubility parameters for the selected polymers, solvents, and nonsolvents [28].

Substance	δ_D	δ_P	δ_H	δ	R_a
PES	19.6	10.8	9.2	24.20	-
N-Methyl-2-pyrrolidone (NMP)	18.0	12.3	7.2	22.96	4.1
N,N-dimethylformamide (DMF)	17.4	13.7	11.3	24.86	5.7
Dimethylacetamide (DMAc)	16.8	11.5	10.2	22.77	5.7
Dimethyl sulfoxide (DMSO)	18.4	16.4	10.2	26.68	6.2
PEG-400	17.88	4.0	13.85	22.97	8.9
PEG-200	17.97	6.06	17.3	25.67	9.9
PVP	21.4	11.6	21.6	32.54	12.9
H_2O	15.5	16.0	42.3	47.81	34.5

The content of PES in the dope was 19% wt. to obtain favorable mechanical strength of the hollow fiber. The remaining content of the polymeric solution was formulated using the approach, described in [29]: DMF content was 25.5% wt., PEG-200—55% wt., and PVP K-90—0.5% wt.

The dope solution was mixed in a round-bottom bulb employing a silicon oil bath. The bulb was equipped with a dynamic double seal stirrer bearing to restrain the solvent loss and water vapor absorption during mixing. The solvent, polymer, and PVP were placed in the vessel, heated up to 90 °C undisturbed, and left for 1 h to swell. During the next two hours, the rotational speed was set to 30 rpm until the polymers dissolved. Afterward, the temperature was reduced to 60 °C, and PEG-200 was added slowly to prevent irreversible phase separation, and the solution was mixed for three hours. The polymeric solution was transfused into the tank, equipped with a water jacket, and left under vacuum for 15 h for degassing at room temperature.

The schematic of the setup is presented in detail in [30]. The dope solution temperature was kept at 25 °C, employing a water jacket, and the solution was supplied using a gear pump to the spinneret. The schematic of the spinneret is described in [31]. Spinnerets with two different internal ring duct diameters were employed: 1.8 and 1.3 mm. The outer bore needle diameter was 0.8 mm. The bore fluid composition was chosen in accordance

with [27]. Water:DMF:PEG-200 ratio was 26:37:37. The air-gap height was 0.2 m, water at 50 °C was used as a coagulation media, and the take-up speed was 5.5 or 11 m/min.

The treatment of hollow fiber bundles, as well as the measurement of internal and external diameters with optical and scanning electron microscopes, are described elsewhere [29]. The bubble point technique was used to characterize the mechanical properties, hollow fiber integrity, and the absence of defects. For this purpose, hollow fibers wet with water were pressurized with nitrogen. The pore size distribution (PSD) was measured by a liquid–liquid displacement porosimetry (LLDP) [32] using porometer POROLIQ 1000 ML (Porometer, Belgium). The procedure is described elsewhere [29].

The atomic force microscopy (AFM) technique was employed for the quantitative analysis of the hollow fiber selective layer morphology. Scanning probe microscope Horiba Smart SPM (France) was used. Scanning of the samples was conducted in the tapping mode. Type PPP-NCYR-20 probes with a radius <7 nm (NANOSENSORS) were employed. Roughness profiles were extracted from 2D AFM images at 45º toward the draw direction. The following roughness parameters were calculated in Gwiddion using ISO 4287-1997: average roughness (R_a), root mean square roughness (R_q), maximum-peak-to-peak-valley height (R_t), mean-peak-to-valley roughness (R_{tm}), mean valley depth (R_{vm}), and mean peak height (R_{pm}).

3. Results and Discussion

In this study, four types of hollow fibers were obtained at similar spinning conditions, with outer and lumen diameters of 1.21 ± 0.01 and 0.76 ± 0.01 mm, respectively. The typical micrograph of the hollow fiber cross-section is presented in Figure 1. The wall thickness was 0.22 mm, and its structure was sponge-like, which is beneficial for the absence of defects and mechanical robustness of the fiber. When the diameter of the spinneret orifice was 1.3 mm, the hollow fiber outer and lumen diameters were almost matching the diameters of the ring duct and the bore needle, respectively. Then, the draw ratio calculated by (1) was equal to 1.2. If the spinneret was employed with the ring duct diameter of 1.8 mm, then the draw ratio was equal to 3.0. Fibers were obtained at two different winding speeds (Table 2).

The pure water permeance varied insignificantly, regardless of the draw ratio or the take-up speed, and was around 1000 L/(m^2·h·bar), i.e., within the experimental error of 5% the permeances were equal. The burst pressure in water (P_{burst}) and butanol/water were, respectively, nearly identical for all samples. Consequently, neither the draw ratio nor the take-up speed affected the mechanical properties and the bulk wall characteristics of the fiber.

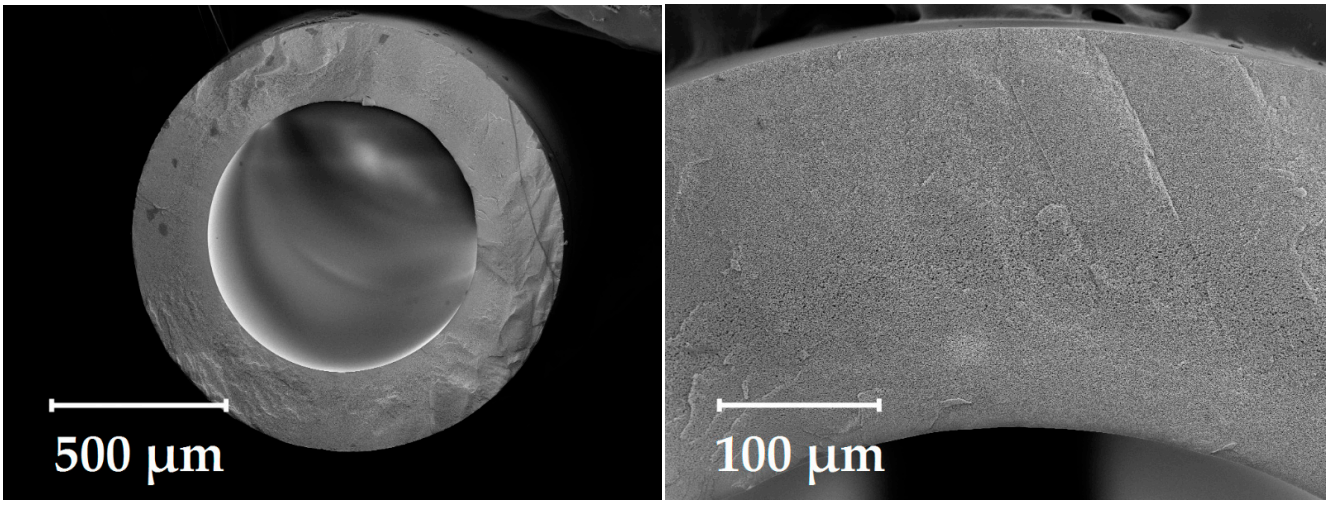

(**a**) (**b**)

Figure 1. SEM micrographs: (**a**) the hollow fiber cross-section; (**b**) zoomed-in image of the wall.

Table 2. The influence of the draw ratio and take-up velocity on the hollow fiber membrane properties.

Sample #	**1**	**2**	**3**	**4**
Draw ratio	1.2	3.0	1.2	3.0
Take-up velocity, m/min	5.5	5.5	11	11
P/l, l/(m^2·h·bar)	1000	950	1020	1030
P_{burst}(H_2O), bar	10	10	10	10
P_{burst} (BuOH/H_2O), bar	4.6	4.6	4.4	4.7
Mean pore size (LLDP), nm	25	33	35	45
Maximum pore size (LLDP), nm	48	54	81	96

All of the obtained samples had limiting pore sizes typical for UF membranes (Figure 2). It is worth noting that, in contrast to a rather typical unimodal distribution, all samples demonstrated at least two peaks at the pore size distribution (PSD) curves. For instance, sample 1 had one noticeable peak near the maximum pore size in the range 38–48 nm and another corresponding to the mean pore size at 25 nm. Samples 1 and 2 obtained at low speed have narrower limiting PSD. An increase in take-up speed had a significant effect on the enlargement of pores: a 40–70% rise in mean and maximum pore sizes was observed for both draw ratios, whereas the shape of the curves obtained at identical draw ratios remained the same.

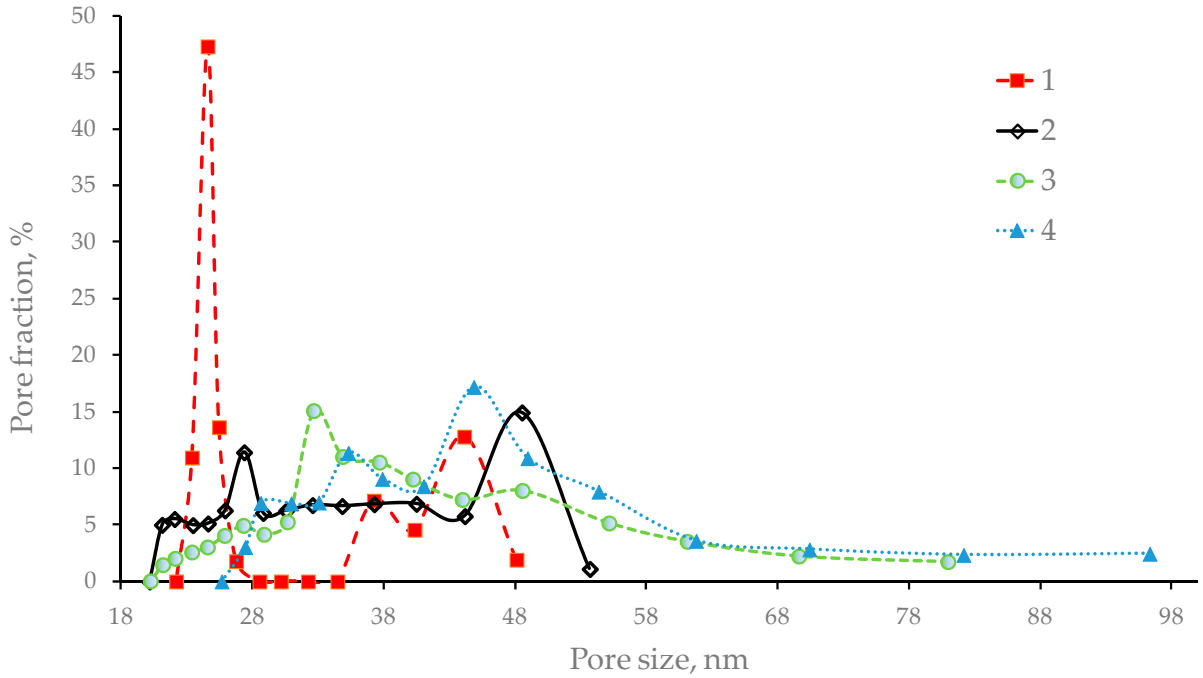

Figure 2. Limiting PSD of hollow fiber membranes obtained at different draw ratios and take-up speed.

A lesser enlargement of 30% was observed in the mean pore size with the rise in the draw ratio, whereas the maximum pore size increase was 10–20%. In the case of draw ratio increase, the shape of the curves obtained at similar take-up speed remained comparable as well.

From the SEM micrographs (Figure 3), a noticeable influence is observed in terms of both the draw ratio and take-up speed on the hollow fiber selective layer morphology. For sample 1, the surface is smooth and homogeneous, and several ledges are seen. With the increase in the take-up speed (sample 3), small stretches started to appear, from which a second phase—namely, the porous sublayer of the membrane, was detected. With the rise in the draw ratio, these stretches expanded in size and covered around half of the micrograph area (samples 2 and 4).

In the NIPS technique, the formation of the selective layer at the lumen side of the hollow fiber is caused by the concentration and vitrification of the polymer at the dope–bore liquid interface. In this study, to suppress the formation of macrovoids, large tear-shaped or spherical pores that compromise the mechanical robustness of the membrane, a solvent was added to the bore liquid. This technique delays phase separation and provides uniform porosity in the bulk of the hollow fiber wall [27,29]. However, it also slows down the vitrification of the selective layer. While the selective layer is not sufficiently solidified, excessive draw causes its stretching and crop-up of the porous sublayer.

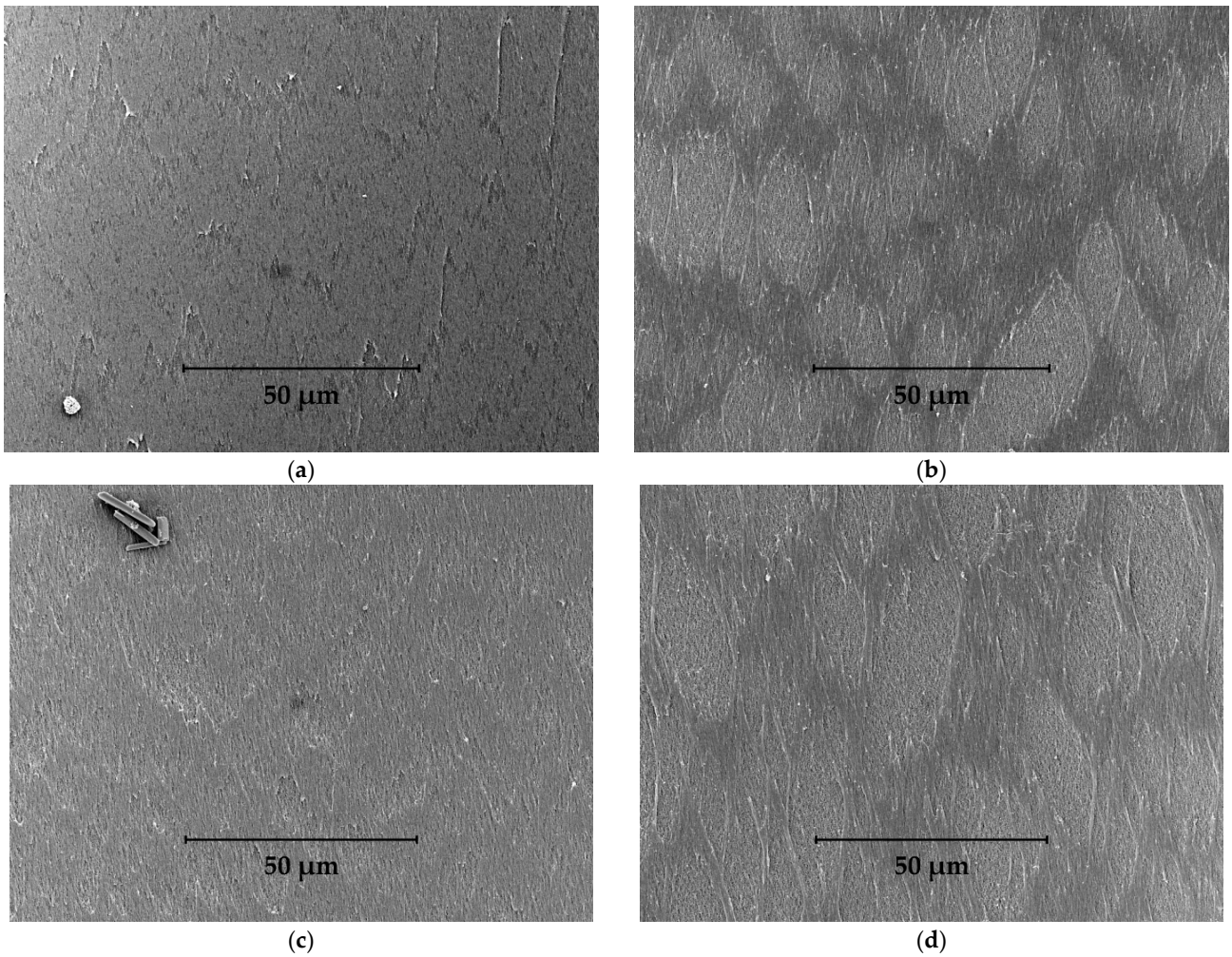

Figure 3. SEM micrographs of membrane selective layer obtained at different draw ratios and take-up speeds: (**a**)-sample 1, (**b**)-sample 2, (**c**)-sample 3, (**d**)-sample 4.

From SEM (Figure 3), 2D (Figure 4), and 3D (Figure 5) topographical images of the membrane selective layer, it was confirmed that the stretches were aligned with the direction of the draw. Surface roughness and inhomogeneity increase were observed with the rise in both the draw ratio and take-up speed (Table 3). From Table 3 and Figure 5, it can be noted that, with an increase in speed, the corresponding rise in roughness (R_a and R_q) was almost twice higher for the sample obtained at a low draw ratio: 40% at DR = 1.2 vs. 20% at DR = 3.0. It should be noted, however, that samples with high DR were already rougher, whereas the gain in roughness parameters indicating the level difference (R_t, R_{tm}, R_{vm}, and R_{pm}) was close to 20% for both draw ratios.

A more significant impact was observed with the increase in the draw ratio. At low speed, a higher draw ratio resulted in a 60–70% rise in the surface roughness, whereas at high speed, the surface roughness increase was 40%. This occurred because, at a higher

speed (sample 3), the starting roughness had already been elevated. The gain in level-difference values was roughly 50% for both high and low speed.

Clearly, the gain in the roughness amplitude was the result of the dense selective layer ("phase 1") stretching, which caused "phase 2"—namely, porous sublayer, to crop up on and become visible from the surface. These two phases were well separated in sample 4. The comparison of images of these two phases taken from sample 4 is presented in Figure 6, and their roughness amplitudes are presented in Table 3.

Table 3. Selective layer roughness parameters.

Sample #	Size, μm	R_a, nm	R_q, nm	R_t, nm	R_{tm}, nm	R_{vm}, nm	R_{pm}, nm
1	35 × 35	17	22	159	109	58	52
3	35 × 35	25	32	195	132	66	66
2	35 × 35	29	36	231	172	96	78
4	35 × 35	35	45	313	192	94	98
4 (phase 1)	3.5 × 3.5	8	11	126	52	28	23
4 (phase 2)	3.5 × 3.5	20	25	178	110	67	51

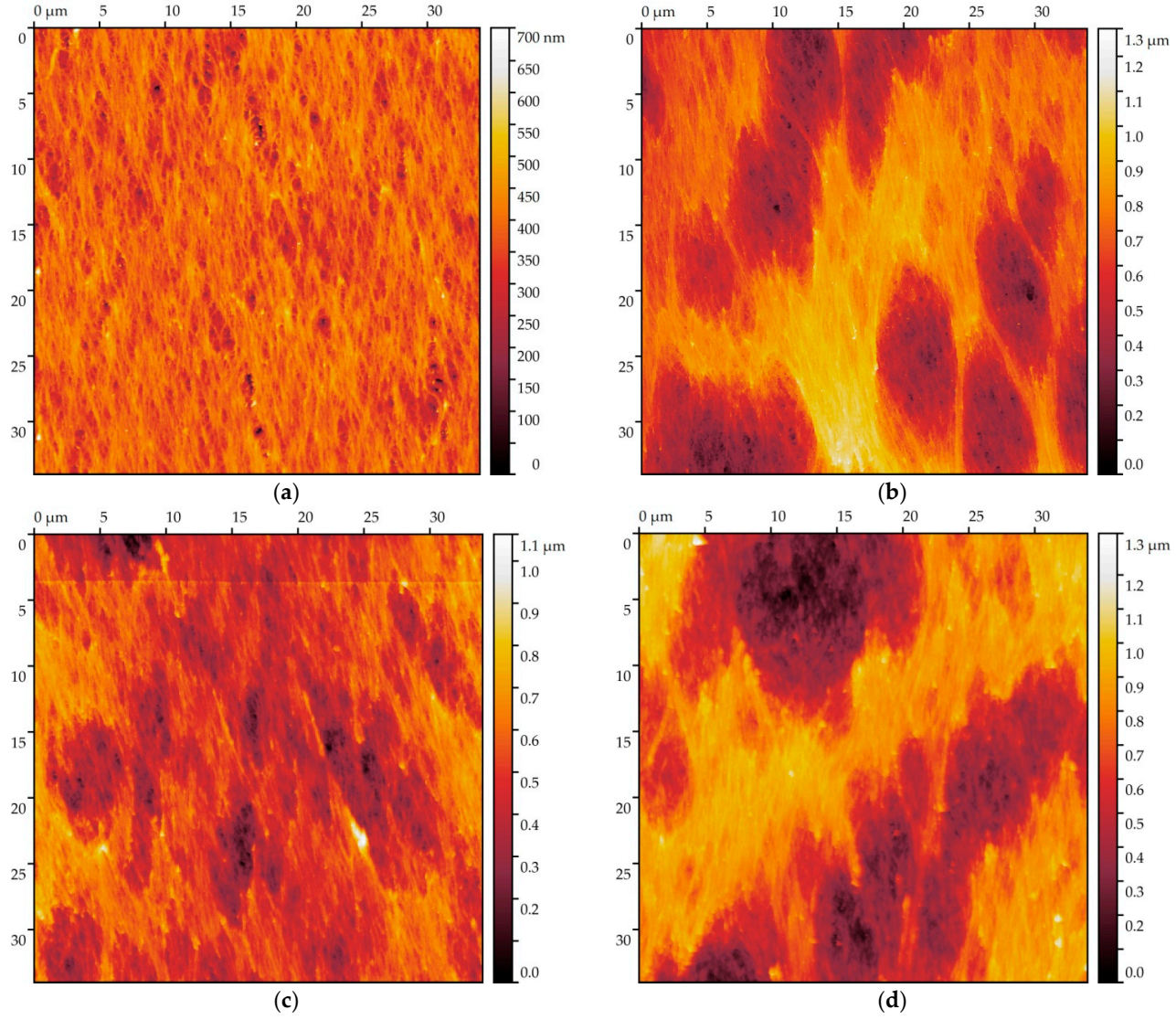

Figure 4. The 2D AFM micrographs of membrane selective layer (top view) obtained at different draw ratios and take-up speeds: (**a**)-sample 1, (**b**)-sample 2, (**c**)-sample 3, (**d**)-sample 4.

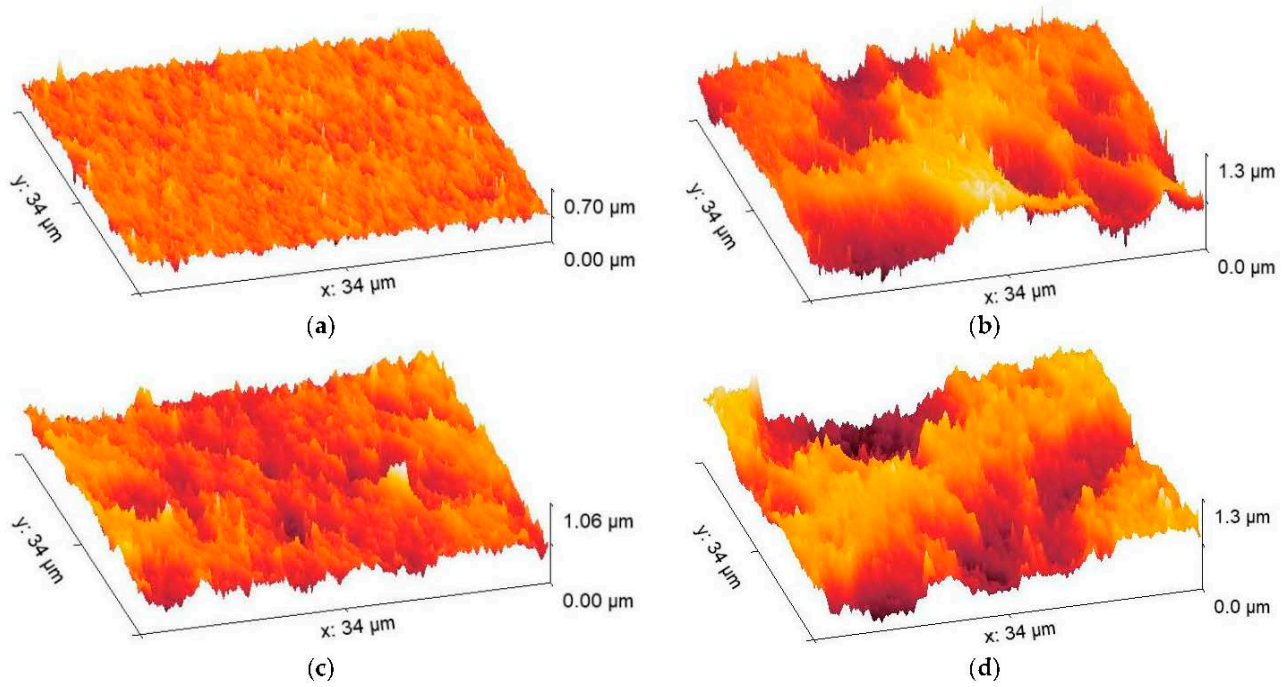

Figure 5. The 3D AFM micrographs of membrane selective layer (top view) obtained at different draw ratios and take-up speeds: (**a**)-sample 1, (**b**)-sample 2, (**c**)-sample 3, (**d**)-sample 4.

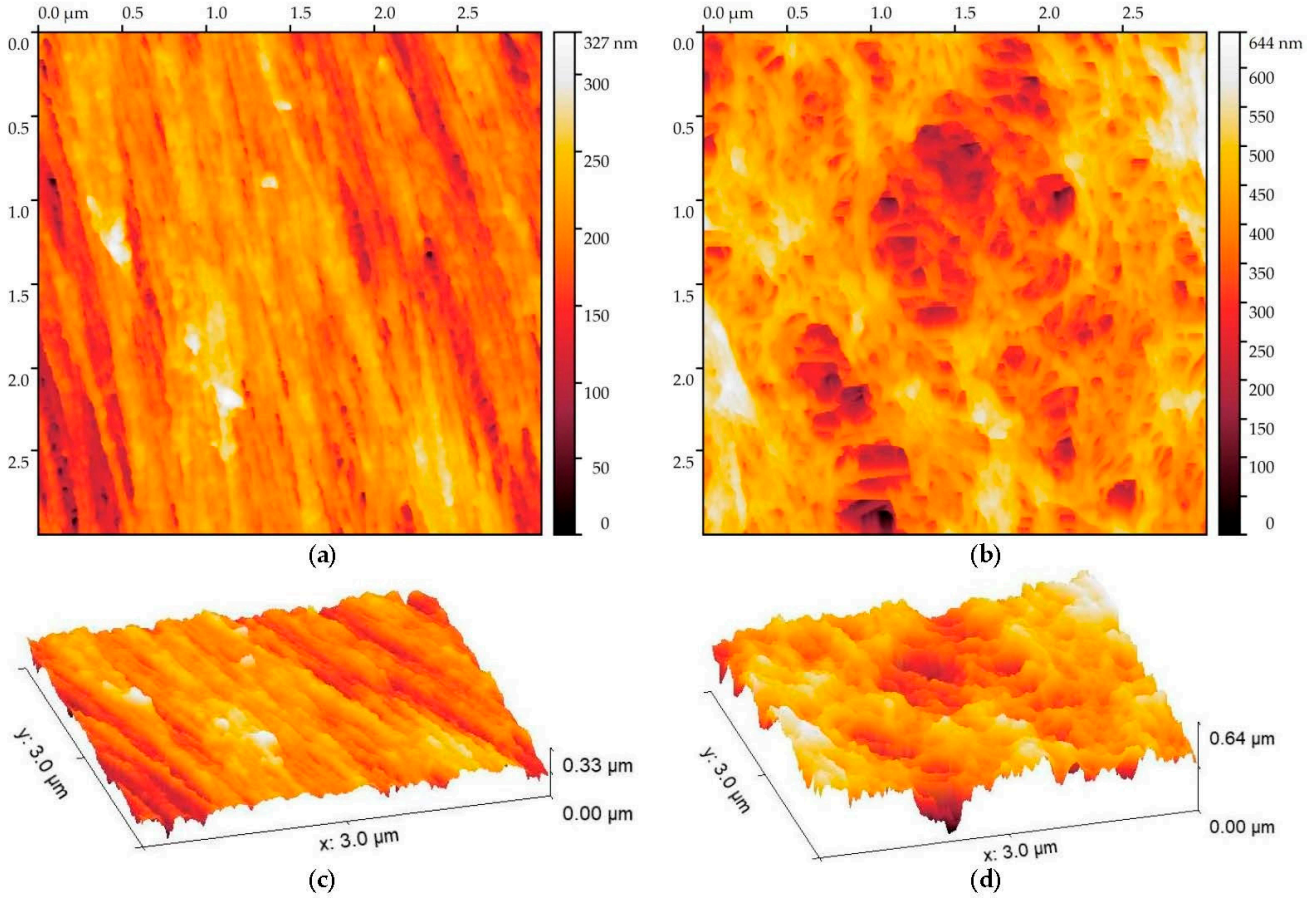

Figure 6. The 2D AFM images of (**a**) the dense selective layer and (**b**) porous sublayer, as well as 3D images of (**c**) the dense selective layer and (**d**) porous sublayer.

The dense selective layer ("phase 1") thickness was 200–300 nm, and it was composed of filaments aligned in parallel, which were, in turn, composed of polymeric spheres connected by slightly thinner bridges. Such spheres are often called "nodules" [33], and their size, as well as the size of the interspacing between them, is around 50 nm. The alignment of nodules in the direction of the draw at the lumen side of the hollow fiber has also been previously reported [34]. Two types of pores are seen on the image: a prevailing number of spherical pores with the same order of size as the nodules, as well as slit-like pores that formed as the interspacing between the filaments, with an effective pore size of up to 100 nm, are also observed. The morphology of "phase 1" is comparable to sample 1, and a similar bimodal pattern is shown by the LLDP measurements of sample 1 (Table 2), suggesting that pores at the surface are cone-shaped. Apparently, pores that had a size of 50 nm on the surface were narrowed down to 25 nm, representing the mean pore fraction, whereas 100 nm surface pore size resulted in a 40–50 nm maximum pore fraction.

The porous sublayer ("phase 2") was also composed of filaments, but in this case, they were not arranged. The roughness was at least twice higher than that in the selective layer but still lower than for samples obtained with high take-up speed (samples 3 and 4) or draw ratio (samples 2 and 4). This suggests that high roughness in these samples is caused not just by the presence of two different phases but rather by the presence of a distinct boundary between them and by the fact that the sublayer is situated at a significantly lower level than the selective layer.

The maximum pore size in the porous sublayer reached 300 nm, whereas the maximum limiting pore size for the samples with the highest roughness (samples 3 and 4) was 80–90 nm (Table 2). Together with the rise in the mean valley depth (R_{vm}), this indicates that the limiting pore diameter moved deeper in the bulk of the wall in comparison with sample 1. The rise in the mean pore size and the content of the large pore fraction on the LLDP PSD (Figure 2) for samples 3 and 4 was related to the crop-up of the porous layer.

It was revealed that the limiting pore sizes were affected more by the change in the take-up speed, whereas the surface pore sizes, roughness, and morphology were controlled by the draw ratio. This observation confirms that with the increase in the draw ratio, the limiting pore sizes shift to the bulk of the wall. They can be further increased by the rise in the take-up speed.

4. Conclusions

In this study, a technique was described to obtain state-of-the-art ultrafiltration hollow fiber membranes from polyethersulfone with the selective layer at the lumen side of the membrane. The pure water permeance was 1000 L/(m^2·h·bar), and the burst pressure in water was 10 bar. To provide uniform porosity along the fiber wall and, consequently, the absence of defects, a solvent was added to the bore liquid. When the draw ratio was close to unity (1.2), and the take-up speed was 5.5 m/min, the selective layer morphology was homogeneous and smooth. It was shown by AFM that the polymeric nodules and filaments were aligned in parallel with the direction of the draw. The mean and maximum pore sizes were 25 and 48 nm, respectively, as measured by the LLDP.

It was shown that neither the draw ratio nor the take-up speed affected the membrane permeance and mechanical properties. The increase in the take-up speed led to the 40–70% enlargement of limiting pores, whereas a 10–30% rise was observed with the increase in the draw ratio. Apparently, while the selective layer was not sufficiently solidified, an excessive increase in the draw caused its stretching and crop-up of the porous sublayer. This led to a drastic increase in selective layer surface roughness and was accompanied by the shift of limiting pore sizes deeper to the bulk of the wall. Limiting pore sizes were affected more by the change in the take-up speed, whereas the surface pore sizes, roughness, and morphology were influenced by the draw ratio.

The UF membrane samples obtained at high speed and, especially, draw ratio, had the following drawbacks: increased roughness, nonuniform morphology, limiting pore size situated deeper in the bulk of the porous sublayer, and deeper valleys. According to the

reported data [19–24], these samples are prone to fouling and show reduced effectiveness of the backwash. For the industrial manufacture of UF hollow fiber membranes, the draw ratio value should be maintained close to unity. To this end, the diameters of the spinneret ring duct and the bore needle should match the fiber outer and lumen diameters, respectively. The take-up velocity should match the average dope extrusion velocity and be as low as practically possible. These measures will help to decrease the fouling rate during the industrial application of UF membranes.

Author Contributions: Conceptualization, G.D.; formal analysis, V.S., S.M., E.G., and A.Y.; funding acquisition, G.D. and V.V.; investigation, G.D., V.S., S.M., and A.Y.; methodology, V.S., S.M., and A.Y.; project administration, G.D. and V.V.; resources, V.V.; validation, G.K.; visualization, G.D. and E.G.; writing—original draft preparation, G.D.; writing—review and editing, G.K., S.M., E.G., A.Y., and V.V. All authors have read and agreed to the published version of the manuscript.

Funding: Measurement of pore size and distribution by LLDP and study of the selective layer morphology by AFM was performed within the frame of the TIPS RAS State program.

Acknowledgments: This research was performed using the equipment of the Shared Research Center, the Analytical Center of Deep Oil Processing and petrochemistry of the Topchiev Institute of Petrochemical Synthesis RAS (TIPS RAS).

Conflicts of Interest: The authors declare no conflict of interest.

References

1. Guillen, G.R.; Pan, Y.; Li, M.; Hoek, E.M.V. Preparation and characterization of membranes formed by nonsolvent induced phase separation: A review. *Ind. Eng. Chem. Res.* **2011**, *50*, 3798–3817. [CrossRef]
2. Bildyukevich, A.V.; Plisko, T.V.; Liubimova, A.S.; Volkov, V.V.; Usosky, V.V. Hydrophilization of polysulfone hollow fiber membranes via addition of polyvinylpyrrolidone to the bore fluid. *J. Membr. Sci.* **2017**, *524*, 537–549. [CrossRef]
3. Qin, J.-J.; Chung, T.-S. Effects of orientation relaxation and bore fluid chemistry on morphology and performance of polyethersulfone hollow fibers for gas separation. *J. Membr. Sci.* **2004**, *229*, 1–9. [CrossRef]
4. Susanto, H.; Ulbricht, M. Characteristics, performance and stability of polyethersulfone ultrafiltration membranes prepared by phase separation method using different macromolecular additives. *J. Membr. Sci.* **2009**, *327*, 125–135. [CrossRef]
5. Idris, A.; Zain, N.; Noordin, M.Y. Synthesis, characterization and performance of asymmetric polyethersulfone (PES) ultrafiltration membranes with polyethylene glycol of different molecular weights as additives. *Desalination* **2007**, *207*, 324–339. [CrossRef]
6. Bildyukevich, A.V.; Hliavitskaya, T.A.; Kavalenka, M.N. The modification of polyethersulfone membranes using a synperonic f108 block copolymer and their application for the fractionation of thermomechanical pulp mill process water. *Membr. Membr. Technol.* **2020**, *2*, 210–216. [CrossRef]
7. Matveev, D.N.; Vasilevsky, V.P.; Kutuzov, K.A. Properties of polysulfone hollow fiber membranes depending on the method of the spinning solution preparing. *Key Eng. Mater.* **2020**, *869*, 443–448. [CrossRef]
8. Wang, K.Y.; Matsuura, T.; Chung, T.-S.; Guo, W.F. The effects of flow angle and shear rate within the spinneret on the separation performance of poly(ethersulfone) (PES) ultrafiltration hollow fiber membranes. *J. Membr. Sci.* **2004**, *240*, 67–79. [CrossRef]
9. Qin, J.-J.; Chung, T.-S. Effect of dope flow rate on the morphology, separation performance, thermal and mechanical properties of ultrafiltration hollow fibre membranes. *J. Membr. Sci.* **1999**, *157*, 35–51. [CrossRef]
10. Qin, J.-J.; Gu, J.; Chung, T.-S. Effect of wet and dry-jet wet spinning on the shear-induced orientation during the formation of ultrafiltration hollow fiber membranes. *J. Membr. Sci.* **2001**, *182*, 57–75. [CrossRef]
11. Tang, Y.; Li, N.; Liu, A.; Ding, S.; Yi, C.; Liu, H. Effect of spinning conditions on the structure and performance of hydrophobic PVDF hollow fiber membranes for membrane distillation. *Desalination* **2012**, *287*, 326–339. [CrossRef]
12. Bildyukevich, A.V.; Hliavitskaya, T.A.; Melnikova, G.B. Structure and properties of polyethersulfone membranes based on polyethersulfone–nonsolvent–solvent systems. *Membr. Membr. Technol.* **2020**, *2*, 283–295. [CrossRef]
13. Bildyukevich, A.V.; Hliavitskaya, T.A.; Pratsenko, S.A.; Melnikova, G.B. The Modification of polyethersulfone membranes with polyacrylic acid. *Membr. Membr. Technol.* **2021**, *3*, 24–35. [CrossRef]
14. Chung, T.-S.; Xu, Z.-L.; Lin, W. Fundamental understanding of the effect of air-gap distance on the fabrication of hollow fiber membranes. *J. Appl. Polym. Sci.* **1999**, *72*, 379–395. [CrossRef]
15. Peng, N.; Chung, T.S. The effects of spinneret dimension and hollow fiber dimension on gas separation performance of ultra-thin defect-free Torlon®hollow fiber membranes. *J. Membr. Sci.* **2008**, *310*, 455–465. [CrossRef]
16. Matveev, D.N.; Kutuzov, K.A.; Vasilevsky, V.P. Effect of draw ratio on the morphology of polysulfone hollow fiber membranes. *Membr. Membr. Technol.* **2020**, *2*, 351–356. [CrossRef]
17. Feng, C.Y.; Khulbe, K.C.; Matsuura, T.; Ismail, A.F. Recent progresses in polymeric hollow fiber membrane preparation, characterization and applications. *Sep. Purif. Technol.* **2013**, *111*, 43–71. [CrossRef]

18. Cao, C.; Chung, T.S.; Chen, S.B.; Dong, Z.J. The study ofelongation and shear rates in spinning process and its effect ongas separation performance ofpoly(ether sulfone) (PES)hollow fiber membranes. *Chem. Eng. Sci.* **2004**, *59*, 1053. [CrossRef]
19. Kumar, R.; Ismail, A.F. Fouling control on MF/ UF membranes: Effect of morphology, hydrophilicity and charge. *J. Appl. Polym. Sci.* **2015**, *132*, 42042. [CrossRef]
20. Sagle, A.; Van Wagner, E.; Ju, H.; McCloskey, B.; Freeman, B.; Sharma, M. PEG-coated reverse osmosis membranes: Desalination properties and fouling resistance. *J. Membr. Sci.* **2009**, *340*, 92–108. [CrossRef]
21. Hoek, E.; Bhattacharjee, S.; Elimelech, M. Effect of membrane surface roughness on colloid–membrane DLVO interactions. *Langmuir* **2003**, *19*, 4836–4847. [CrossRef]
22. Hashino, M.; Katagiri, T.; Kubota, N.; Ohmukai, Y.; Maruyama, T.; Matsuyama, H. Effect of membrane surface morphology on membrane fouling with sodium alginate. *J. Membr. Sci.* **2011**, *366*, 258–265. [CrossRef]
23. Hashino, M.; Katagiri, T.; Kubota, N.; Ohmukai, Y.; Maruyama, T.; Matsuyama, H. Effect of surface roughness of hollow fiber membranes with gear-shaped structure on membrane fouling by sodium alginate. *J. Membr. Sci.* **2011**, *366*, 389–397. [CrossRef]
24. Gohari, R.; Lau, W.; Matsuura, T.; Ismail, A. Effect of surface pattern formation on membrane fouling and its control in phase inversion process. *J. Membr. Sci.* **2003**, *446*, 326–331. [CrossRef]
25. Ivanov, M.V.; Dibrov, G.A.; Loyko, A.V.; Varezhkin, A.V.; Kagramanov, G.G. Techniques to manage geometry characteristics of hollow fiber membranes. *Theor. Found. Chem. Eng.* **2016**, *50*, 316–324. [CrossRef]
26. Ma, Y.; Shi, F.; Ma, J.; Wu, M.; Zhang, J.; Gao, C. Effect of PEG additive on the morphology and performance of polysulfone ultrafiltration membranes. *Desalination* **2011**, *272*, 51–58. [CrossRef]
27. Liu, Y.; Koops, G.H.; Strathmann, H. Characterization of morphology controlled polyethersulfone hollow fiber membranes by the addition of polyethylene glycol to the dope and bore liquid solution. *J. Membr. Sci.* **2003**, *223*, 187–199. [CrossRef]
28. Hansen, C. *Hansen Solubility Parameters: A User's Handbook*, 2nd ed.; CRC Press: Boca Raton, FL, USA, 2007; 544p.
29. Dibrov, G.; Kagramanov, G.; Sudin, V.; Grushevenko, E.; Yushkin, A.; Volkov, A. Influence of sodium hypochlorite treatment on pore size distribution of polysulfone/polyvinylpyrrolidone membranes. *Membranes* **2020**, *10*, 356. [CrossRef]
30. Dibrov, G.; Ivanov, M.; Semyashkin, M.; Sudin, V.; Kagramanov, G. High-pressure aging of asymmetric Torlon®hollow fibers for helium separation from natural gas. *Fibers* **2018**, *6*, 83. [CrossRef]
31. Dibrov, G.; Ivanov, M.; Semyashkin, M.; Sudin, V.; Fateev, N.; Kagramanov, G. Elaboration of high permeable macrovoid free polysulfone hollow fiber membranes for air separation. *Fibers* **2019**, *7*, 43. [CrossRef]
32. Zeman, L.J.; Zydney, A. *Microfiltration and Ultrafiltration: Principles and Applications*, 1st ed.; Marcel Dekker: New York, NY, USA, 1996; pp. 197–201.
33. Khulbe, K.C.; Feng, Y.; Matsuura, T. Nodular structure of polymers in the membrane. In *Synthetic Polymeric Membranes*; Pasch, P., Ed.; Springer: Heidelberg/Berlin, Germany, 2008; pp. 47–100.
34. Khulbe, K.; Feng, C.; Matsuura, T.; Kapantaidakis, G.; Wessling, M.; Koops, G. Characterization of polyethersulfone-polyimide hollow fiber membranes by atomic force microscopy and contact angle goniometery. *J. Membr. Sci.* **2003**, *226*, 63–73. [CrossRef]